Planar Near-Field Measurements on Radiometer Antennas up to 183 GHz for the Global Precipitation Measurement Satellite

Andrew Shroyer, Ray Lovestead and Eric Darnel
Ball Aerospace Corporation
1600 Commerce St
Boulder, CO 80301

Allen Newell
Nearfield Systems Inc.
19730 Magellan Drive
Torrance, CA 90502

ABSTRACT

The Global Precipitation Measurement (GPM) mission is a satellite based Earth science mission that will study the global precipitation from rain, ice and snow. A critical part of this satellite is the multi-frequency radiometer system that covers frequencies up to 183 GHz. Beam pointing and beam efficiency must be measured very accurately to calibrate the radiometer response. This paper will focus on the measurements of the offset reflector antenna operating up to 183 GHz using a Nearfield Systems Inc. (NSI) planar near-field measurement system and the special challenges that this presents. Results will be presented and the uncertainty in beam pointing will be discussed.

Keywords:

1. Introduction

The GPM Microwave Imager (GMI) instrument is a conical scanning microwave radiometer that serves as both a precipitation standard and as a radiometric standard for other GPM constellation members. The GPM radars will be used to accurately measure, via reflectivity and estimates of attenuation, the vertical profiles of the clouds and precipitation, including the drop size distribution.

The GMI contains thirteen microwave channels ranging in frequency from 10 GHz to 183 GHz. The GMI 1.2m main reflector carries 4 channels about the 166/188 GHz bands that provide significantly improved spatial resolution over previous precipitation measurement missions. It is these bands that present beam pointing and characterization challenges.

The unique challenges of measuring a satellite instrument in situ will be discussed with regards to assembly within a clean room. Selecting RF absorber that functions from 10 GHz to 200 GHz will be studied with recommendations made. Uncertainty in beam pointing will be developed based on a 19- term analysis error analysis.

2. Near-field Scanner Setup

A near-field scanner was selected over a far-field range to allow antenna measurements throughout the duration of construction without significantly interfering with schedule. In the past, compact ranges were used and required multiple months to build, align, measure and fine tune the beam pointing of the antenna system. All of this offsite work would impede the construction progress of the instrument. Using an onsite scanner, near-continuous measurements are taken as the build progresses.

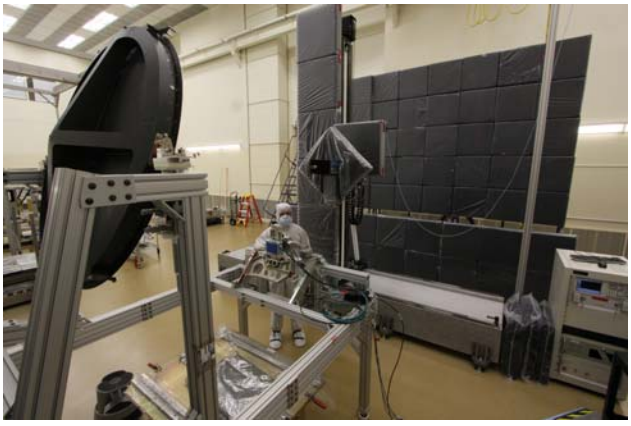

Figure 1 Photo of the GMI Reflector and near-field scanner

The 12’ wide x 9’ high planar scan area was selected to encompass both the main beam of the main reflector in its inherent Main Reflector Coordinate System (MRCS, orthogonal to the plane of the scanner) and the main beam in its satellite configured state (tilted 45° below horizon). Accurate antenna alignment to the 12x9 scanner is a non-trivial affair that requires use of a laser tracker to assure repeatable measurements. The reflector and its feed

assembly must be aligned to the satellite and the near field scanner. Room targets provide a fixed coordinate system that is used to re-assess alignment from time to time.

A pair of OML V05VNA2-T/R mm-wave extender modules are used to up and down convert to and from 183 GHz. Mountings for the extender modules must be made accurately to assure rotational symmetry and probe pointing precision.

3. Absorber Selection/Clean Room

Operating in a class 10,000 clean room from 10 GHz to 183 GHz does not present any particular challenges for the scanner equipment itself. It is the RF absorber around the scanner tower, probe and nearby walls that present a real problem. Carbon loaded foam creates a mess as the material degrades over time. Several absorber manufacturers produce class 100,000 rated blocks, which while close, is not good enough.

In order to get RF absorber blocks into a clean room we must be able to wipe them down and inspect for any particulate. This is impossible with any type of untreated foam blocks. Some manufacturers have taken to encapsulating the absorber in Styrofoam and others are trying a rubberized paint. All of these solutions suffer from poor performance at higher frequencies. Coatings reduce the absorber's match and flat surfaces look like near perfect mirrors at higher frequencies.

The solution to produce class 10,000 absorber is to use thin plastic bags to enclose each block. The emphasis on thin is due to the fact that even 1 mil of plastic presents significant enough material for mismatch. We found that tautly stretching a piece of 1mil Kapton sheet would cause the reflected rays to coherently return back to the antenna under test. Therefore, when using plastic bags, utilize the thinnest possible bags (<0.5mil) and do not allow the bagged absorber wall to present a large flat surface to the incoming wave.

A primitive 2-port absorber laboratory was set up to measure the reflected signal strength of our chosen absorber with various wrappings. Two OML V05VNA-T/R modules were arranged with two medium gain horn antennas. They were placed to approximate a direct, orthogonal wave front to the absorber under test. Separations of 30 and 60 degrees were also tested, with very similar results. An aluminum plate was used as both a backing and reflection coefficient reference. Results are presented in Table 1.

Pyramidal carbon loaded foam is still the most common absorber design. High frequency performance modifications such as varying the tip height in a random fashion and using an egg-crate (so called convoluted) shape help improve absorption up to and above 40 GHz. But at 183 GHz the wavelength is ~0.06" and the mere presence of the typical blue paint can affect the absorptive properties.

Table 1 Foam absorber reflectivity tests at 183 GHz

Foam absorber configuration	Reflectivity
Styrofoam encapsulated 6" pyramidal	-10dB
6" thick flat rectangular block	-23dB
3" convoluted "egg crate" blue coated	-33dB
6" standard pyramidal	-40dB
6" thin rubber coated pyramidal	-37dB
4" AEMI AEC-4/1-MM-HP	-40dB

We have discovered that any foam absorber performs poorly above 100 GHz and that the best we can expect is for the impinging RF wave front to be randomly scattered from the absorber and combine coherently back at the probe with a very low probability. Interestingly, the 3" convoluted absorber did not perform as well as 6" pyramidal foam. This is most likely due to the fact that the 3" convoluted foam was relatively flat in comparison to the 6" pyramids. Also, the rubber coated pyramidal foam only performed slightly worse than the uncoated foam. This is due to the scattering pattern shape from the absorber shape and not due to the carbon loaded foam characteristics. The rubberized pyramidal absorber would make a decent choice, but the coating process did not cover the back of the absorber and it was not clear if the surface was truly "clean" by visual inspection.

A panacea does not exist for a class 10,000, 10-183 GHz absorber. A compromise was made to use unpainted, convoluted carbon loaded 4" absorber. This provides enough thickness to function well down at 10 GHz and still provides a decent surface at ~100 GHz. AEMI makes a 4" absorber that is stated to perform well up to 75 GHz. AEMI AEC-4/1-MM-HP was chosen for use on all large surfaces (walls, scanner, etc.).

Figure 2 illustrates the effect that the clean room bagging has on the absorber. AEMI absorber was used as a reference for this test. The absorber was tested with thin Kapton (2mil) sheet, thin (0.3mil) polyethylene garbage bags and thin crinkled up poly garbage bags. Also shown is a Styrofoam encapsulated pyramidal absorber. The flat surfaces of the Styrofoam and thick Kapton sheets perform very poorly. The thin garbage bags perform adequate when pulled taut across the surface and is nearly non-existent when crinkled up in a random fashion.

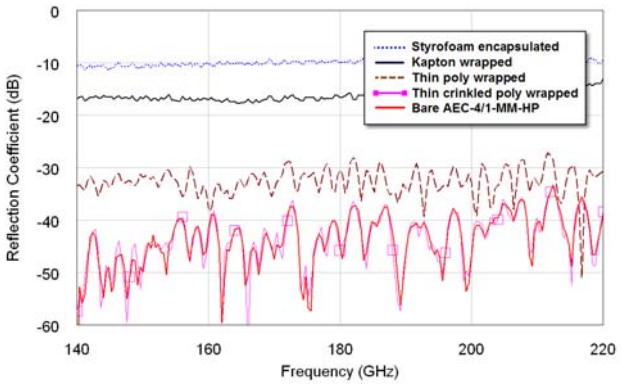

Figure 2 Reflectivity graph AEC-4/1-MM-HP with various wrappings

The single most important piece of absorber is positioned directly behind the probe. Low to medium gain probes have large back lobes that must be reduced to assure that we are not introducing a component which degrades the known probe's relative pattern. Particular care in selecting this piece of absorber will go a long way to ensuring proper pattern measurements. At 183 GHz we use a specially designed high performance black body target produced by Zax Microwave. This is the same carbon loaded dielectric that is used for the hot load reference absorber.

Figure 3 Photo of Zax carbon loaded dielectric absorber behind 140-220 GHz horn

4. Main Beam Pointing Direction Measurement Uncertainty

The GMI antenna beam pointing specification requires the beam location measurement uncertainty to be less than 120 arc seconds (.0333°). The GMI beam location is determined by measurement with a near-field scanner whose orientation to the Main Reflector Coordinate System (MRCS) has been measured with a Laser Tracker. A Fourier transform, implemented using the commercial software NSI2000^{TM}, of the near-field measurements yield the beam pointing direction in the near-field scanner coordinate system. Alignment measurements of optical reflector targets on both the main reflector and of near-field scanner positions provide data for registering the near-field antenna measurements in the MRCS. Sources of error in near-field scanner measurements as outlined in [1] are analyzed and compared to the GMI requirement. This analysis is done for GMI channels 12 & 13 (the 183 GHz band).

To influence beam direction, an error must affect the linear phase slope of the near-field data over the aperture. Reference [1] lists 18 possible sources of error in near-field antenna measurements. An additional term 19, "Transform resolution", was added to those listed in [1]. This is not a theoretical error source, but a practical one arising from a finite angle-space grid that far-field patterns are calculated on.

Table 2 Error terms that will affect beam pointing uncertainty

Error Source	Primary Evaluation Method
AUT alignment error	Measurement
Data point spacing (aliasing)	Computer Simulation with measured data
System phase error due to:	
Flexing cables/rotary joints	Measurement and computer simulation
Temperature effects	Measurement
Room scattering	Measurement
Leakage and crosstalk	Measurement
Random errors in amplitude/phase	Measurement
Transform Resolution	Analysis

AUT Alignment Error

To relate the near-field measurement of beam pointing direction in the MRCS, 3 optical targets on the main reflector were characterized, as well as a 7x7 grid of 49 points in the near-field scan plane by the Laser Tracker. The Spatial Analyzer software used with this instrument allowed the expression of the 7x7 grid directly in the MRCS, since the three points on the reflector had known positions in the MRCS. The 7x7 near-field scan plane spanned 144"x108" (horizontal x vertical) with regular grid spacing. The positions on the 7x7 grid were not recorded in the near-field coordinate system, so an ideal assumption of this grid was used.

A Rayleigh distribution is expected and therefore the variance of the Cartesian angular errors is known from the mean of the Rayleigh distribution. This leads to the standard deviation of the angular errors as 0.0015°.

The probe z-position errors of the 49 test points may be inspected in a similar manner. The mean z-error is about 0.001", or about $\lambda/64$ (5.6°) at 183 GHz. These z-position

errors have the effect of producing an error beam that detracts from an error-free beam. If the errors are independent of one another, then the error beam assumes and isotropic shape that is much lower than the main beam and will not visibly interfere with the pointing direction. This effect is therefore dismissed.

Data Point Spacing
Reference [1] indicates that, for near-boresight antenna patterns, alias-free antenna patterns may be measured using measurement grid spacing approaching 1 λ. The GMI near-field measurements were performed using grid spacing on this order, and therefore are alias-free.

System Phase Errors
Test system phase errors may arise from several sources including:

a.) Cable flex & rotary joints
For the GMI near-field testing, the cables were arranged to minimize changes in stress over the scanning area. Phase drift due to gravitational sag after installation was noticeable at 183 GHz, so tests were conducted after sufficient time elapsed to allow cabling to settle. The main LO cable on the scanner side runs through two rotary joints and has a 14' high service loop. This is the optimum setup; however this cable still has some effect on measurements. Figure's x, y, and z show the results of a test to characterize effects of the cable flex and rotary joint. The test involved installing a very long semi-flex cable between the scanner and the receiver. The semi-flex cable bends very slowly as compared to the LO cable loops on the scanner. The semi-flex cable in this configuration should be fairly stable and the phase variation should be driven by the range cables and rotary joints.

The cable tests were performed at 18.7 GHz. The measured phase variation is 1.5° in the horizontal plane over 140" and 1.0° in the vertical plane over 100". Taking the phase variation to be linear with frequency equates to a 14.7° vertical and a 9.8° horizontal variation at 183 GHz. These are now scaled for the smaller acquisition plane size at 183 GHz of 25", which results in approximately 2.5° horizontal and 2.5° vertical variation. A repeatability plot is included to show the effects due to the cable and rotary joint are well behaved and not random.

The phase slope at 183 GHz due to cable/slip joint variation is 2.5°/25"=0.10°/in. Applying a small angle approximation, this can be taken to be the transverse wave number of the beam calculated from near-field data that includes this error. The axial free-space wave number at 183 GHz is ~5580°/in. These transverse and axial components form a triangle with pointing error angle of 0.0010°.

b.) Drift due to temperature changes
Due to the very short wavelength at the test frequency of 183 GHz (0.065"), phase drift of the test set over the duration of a near-field scan may be considerable. It is critical to allow both the receiver and the OML heads to sufficiently warm up (2-3 hours). Wild phase changes (over 100 degrees) over time will be seen as all the equipment comes up temperature. As an example, the rear receiver rack door was accidentally closed during a test and the phase began to radically climb. To reduce temperature changes the scanner is mounted on a large granite block which helps maintain a constant temperature near the scanner. Also, the clean room has a very stable and monitored temperature.

At 183 GHz, a full single-pol near-field scan required about 6 hours. The measured phase drift rate is about -0.5°/hour. To assess the effect of measurement phase drift, a phase dependence of an ideal equivalent Gaussian aperture field distribution is modified to mimic or amplify the effect of measured phase drift. The near-field measurement used a bidirectional scan that tends to cancel phase drift in 'scan axis'. The effect of phase drift, if it is slow enough compared to the time of a scan slice, is to steer the beam in the plane of the 'step axis'.

Table 1 lists the effects upon the beam pointing direction for a range of linear phase drift rates. Notice that the value corresponding to phase drift measurements yields a change in the step axis direction of 0.0007°. This value is taken to be the beam pointing uncertainty due to phase drift.

We note that even severe phase drift rates have negligible effect upon the beam direction along the 'scan axis' for a bi-directional near-field scan. Further, the NSI2000™ software has an option to sample a fixed point and use this as a phase reference throughout the test. The scanner will periodically sample this point and assume that the phase/amplitude will not change with time and thus calibrate out any temperature drift.

Table 4 Beam Pointing Change for Phase Drift Rates

Phase Drift Rate	Beam Azimuth	Beam Elevation
0°/hour	0.0000°	0.0000°
-0.5°/hour	0.0000°	0.0007°
-5°/hour	-0.0001°	0.0137°
-50°/hour	-0.0000°	0.1481°

Room Scattering
Scattering due to the test fixture, near-field scanner, or other objects appear in the far-field pattern as specular

artifacts. Utilizing absorber on all potential scattering surfaces reduces these artifacts. Absorber selection was addressed in Section 3 of this paper. Correctly reducing scattering levels makes it highly unlikely that room scattering could produce both the level and direction required to visibly interfere with beam pointing.

Quantifying the level of error is done by shifting both the AUT and probe in x, y and z directions and evaluating the delta between them. In our case, moving the AUT multiple times was not a reasonable task considering the time it takes to re-align. Therefore this analysis was not completed.

Leakage and Cross-Talk

Signal leakage through cables, circuits, and electrical components can interfere with the near-field measurements. The NSI system was designed and installed utilizing proven design techniques to minimize leakage. A leakage verification test was done and shows that there were no appreciable leakage signals present. Any leakage signals are at or below the noise floor. Given this test results the effect of leakage on beam pointing is dismissed. **Error! Reference source not found.** shows the 2D scan data of a leakage test. These data show no correlated signal trends expected from leakage. The levels shown are unreferenced.

Random Errors

At the beam center, at 183 GHz, the S/N ratio was 42 dB. To assess what effect this has on beam pointing knowledge, assigned levels of noise were added to the ideal Gaussian beam distribution. Calculated beam pointing angles from a number of independent cases give knowledge of the beam pointing variance.

SNR levels from 40 to 80 dB were assigned to the 183 GHz Gaussian aperture distribution 50 times to accumulate statistical characterization. Figure 5 shows the results of this simulation.

The finite (0.002°) grid sampling of the far-field pattern in this simulation artificially limits the pointing error results, so the curve of Figure 5 may be taken to be an upper limit. For an SNR of 42 dB, the RMS pointing error was 0.00057°.

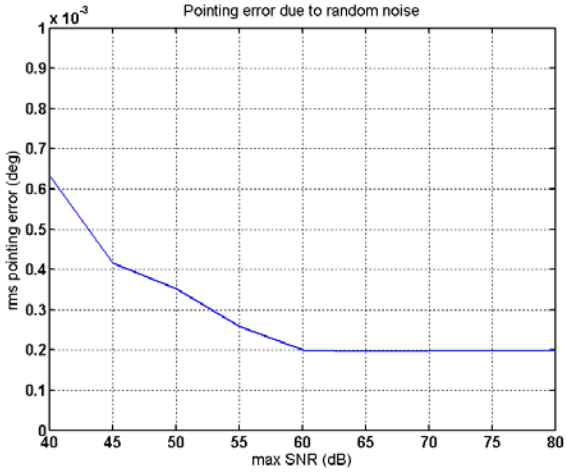

Figure 13 Pointing error due to measurement noise

Transform Resolution

The far-field patterns are calculated on a regular azimuth/elevation grid from which beam pointing is determined. The beam point direction is found by taking the mean of the half-power azimuth/elevation contours. This method produces pointing resolution approximately 10 times finer than the grid angle spacing. In theory, this may be set to an arbitrary low level, but in practice the far-field grid is set to some practical level for tolerable near-field/far-field transform times. The GMI near-field/far-field transforms used various grid spacings, but a spacing of 0.03° was typical. This spacing corresponds to a pointing uncertainty of about 0.003°.

Error Source Summary

The sources of error and their assumed or expected RMS magnitudes are shown in Table 5.

Table 5 Error source summary

Source of Error	RMS error level
AUT alignment error	0.0015°
Data point spacing (aliasing)	0°
System phase errors	
Cable/Rotary Joint Phase	0.0010°
Temperature Phase Drift	0.0007°
Room Scattering	0°
Leakage and crosstalk	0°
Random errors	0.00057°
Transform Resolution	0.003°
RSS Combination	0.0036°

3σ Combined uncertainty	0.0108°

The 3σ uncertainty level is 0.0108° (38 arc seconds). The GMI antenna pointing specification requires the boresight measurement uncertainty to be less than 120 arc seconds

(.0333°). The expected beam pointing uncertainty is well below the required maximum.

5. Measured Beam Pointing

This section provides a brief description of the measured results at 10.65 GHz and 183 GHz, the low end and high end of the GMI operating band. Along with the previously discussed beam pointing requirement, key performance requirements are beam efficiency, half-power beamwidth, and circularity. The antenna characterization data will be used for verification of system level requirements as well as for the instrument calibration.

The near field measurements were recorded and the data was converted to the far field using the software NSI2000TM and then exported to MATLABTM to perform additional analysis. Figure 14 shows the near-field measured patterns and the corresponding transformed far-field. Probe pattern de-convolution is performed during the transform. The scan plane size is such that all relevant power in the forward scene is captured by the near field scanner. By design, the beams are not perfectly orthogonal to the near field scan plane. The beam tilt is evidenced by the near field phase distribution and the peak of beam angle in the far field plots.

The dynamic range and phase stability of the near field system restricts accuracy at the high frequency. The dynamic range at the high frequency is limited by the transmit power available out of the high frequency mixers. A narrow IFBW (high averaging) was used to enhance the signal to noise ratio, and the resulting near field dynamic range achieved was approximately 42 dB at 183 GHz.

Beam efficiency is defined as the power (co-pol) contained in 2.5 half-power beam widths divided by the power (co-pol and x-pol) over all space. In a planar measurement of this type, the back lobe, or spillover lobe, is not characterized and therefore must be accounted for separately. For this application, theoretical back-lobe efficiencies were calculated using physical optics code [2] and applied as described in [3]. The measured results are presented in table 6. The 183 GHz predicted efficiencies contain a budget item due to the negative impact of physical surface accuracy of the main reflector and sub-reflector. The measured RMS surface error of each is on the order of 0.0005", which is approaching the mechanical measurement accuracy, and therefore the predicted efficiency is believed to be somewhat pessimistic.

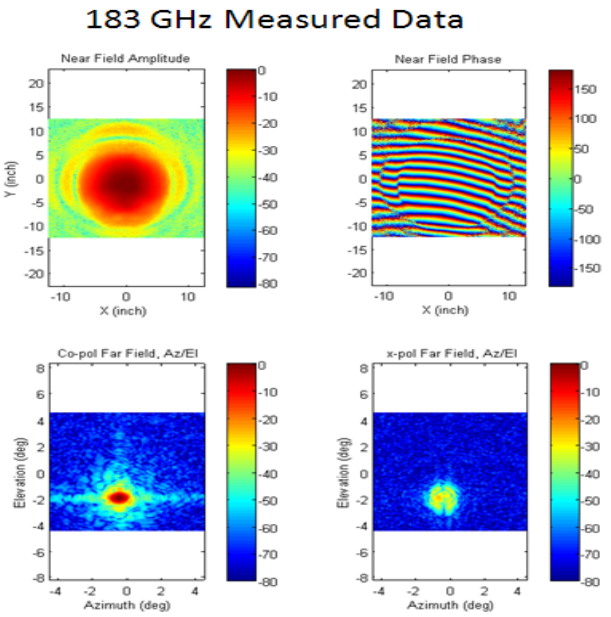

Figure 15 Measured 183 GHz GMI antenna pattern performance

Table 6 Measured Results

	10 GHz		183 GHz	
	Predicted	Measured	Predicted	Measured
Beam Efficiency (Forward-Region)	97.00%	97.30%	96.40%	97.30%
Beam Efficiency*	92.10%	92.60%	95.30%	96.20%
Beamwidth	1.73	1.73	0.39	0.39
Circularity	3.60%	3.70%	7%	12.50%
* contains theoretical all-space fraction				

The principal plane cuts shown in figure 16 compare the theoretical patterns generated using physical optics and the measured patterns. Good agreement is shown. The measured 183 GHz sidelobe levels are higher than what was predicted. This is due to a cowling that was installed on the sub-reflector feed assembly that was not included in the model.

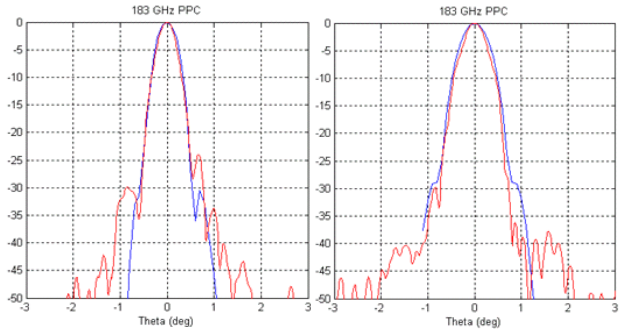

Figure 16 Measured principal plane cuts at 183 GHz

6. Conclusions

Flight RF testing of the GMI radiometer antenna in the near field range is currently underway. The measurement techniques and the near field test range have been shown to be effective for the purposes of characterizing the antenna at frequencies up to 183 GHz. The system repeatability, sensitivity, and accuracy have proved adequate for meeting the antenna characterization knowledge requirements.

The complications brought on by performing these tests in a clean room centered mostly on the absorber. The problem was exacerbated by the fact that the absorber must operate well at high frequencies. Tests showed that adequate results could be obtained by careful selection of the type of absorber as well as the material chosen to enclose it.

The near field range proved to be a convenient way to quickly and accurately characterize a radiometer antenna. Since the AUT does not rotate, precise co-alignment of the reflector to the feed tray can be more easily maintained for large test articles. The near-field range also provides a straight-forward platform for performing precision alignment. Future measurements will continue to validate the range and measurement techniques.

Reference

[1] A. Newell, "Error Analysis Techniques for Planar Near-field Measurements," IEEE Transactions on Antennas and Propagation, June 1988

[2] L. Diaz and T. Milligan, Antenna Engineering Using Physical Optics: Practical CAD Techniques and Software, Artech House Publishers, September 1996.

[3] B. Fischer and I. Lahie "The Spillover Effect on the directivity calculation of reflector antennas in planer near-field measurements", IEEE Antennas and Propagation Magazine, December, 2009, pp 124